Nature of Electrical Junction at the TiO_2/Substrate Interface for Particulate TiO_2 Film Electrodes in Aqueous Electrolytes

Akira Shiga, Akira Tsujiko, Tomohiro Ide, Shinji Yae, and Yoshihiro Nakato*

Department of Chemistry, Graduate School of Engineering Science, and Research Center for Photoenergetics of Organic Materials, Osaka University, Toyonaka, Osaka 560-8531, Japan

Received: February 25, 1998; In Final Form: May 12, 1998

Particulate TiO_2 film electrodes in aqueous electrolytes show photocurrent−potential curves similar to those for single-crystal n-TiO_2 electrodes, though the TiO_2 particles are insulating and simply deposited on conductive substrates without making any ohmic contact. The reason for such an apparently curious phenomenon has been investigated by examining the effect of changing the work function of the substrate ($e\phi_w$). The onset potential of photocurrent (U_{on}) for particulate TiO_2 film electrodes remains nearly the same, irrespective of $e\phi_w$, indicating that a simple Schottky junction model cannot be applied to the TiO_2/substrate contact. On the other hand, the deviation (ΔU) of U_{on} from the flat-band potential of single-crystal n-TiO_2 electrodes (U_{fb}) is nearly zero in the presence of ethanol, but large in the absence of it, especially in acidic solutions. The large ΔU implies that a photocurrent starts to flow by a positive shift of the electrode potential from U_{fb} or, in other words, by formation of certain band inclination in some TiO_2 particles. Two plausible models, extended Schottky junction and Bardeen-type junction, are proposed for the electrical junction at the TiO_2 particle/substrate interface, and it is suggested that the Bardeen-type junction is more plausible, explaining all the experimental results.

Introduction

It is well-known that n-TiO_2 semiconductor electrodes are chemically stable and can photooxidize water into oxygen and H^+ ions under anodic bias.[1] Recently, nanometer-sized TiO_2 particles and their films have attracted growing attention from viewpoints of cleaning of the earth's environment by photodecomposition of pollutants and harmful bacteria[2−23] and of solar energy conversion by dye sensitization solar cells.[24−31]

We have thus far studied in detail the mechanism of photooxidation reaction of water on single-crystal n-TiO_2 (rutile) electrodes in aqueous electrolytes.[32−34] The main conclusion is that surface Ti−OH cannot be oxidized by photogenerated holes, and thus certain active surface sites, such as Ti−OH in atomic gaps exposed to the surface[33,34] and deprotonated Ti−O^- species at the surface, are necessary for the reaction to proceed efficiently. The Ti−OH in atomic gaps can act as an active site because the Ti−OH is mainly stabilized by electronic polarization of the TiO_2 crystal and has a much smaller activation energy for electron transfer (oxidation) than the surface Ti−OH group which is stabilized by orientational polarization of polar solvent (water) molecules in solution.[33−35] The above conclusion for single-crystal n-TiO_2 electrodes will be applied to photoreactions on particulate TiO_2 electrodes. Thus, we have started comparative studies of the reaction mechanism on single-crystal n-TiO_2 with that on particulate TiO_2.

Although many studies have been reported on dye-sensitization photocurrents for particulate TiO_2 film electrodes, there are only a few reports on photocurrents caused by hole oxidation of solution species.[3,19−23] The most surprising result for the particulate TiO_2 electrodes in aqueous electrolytes is that they show photocurrent−potential curves quite similar to those for single-crystal n-TiO_2 electrodes,[32−34] though the TiO_2 particles are almost insulating and simply deposited on conductive substrates without making any ohmic contact, and moreover, the electrolyte solution penetrates into the particulate TiO_2 films and is in direct contact with the substrate.

The present work has thus been done with an aim at clarifying what type of electrical junction is formed at the substrate/TiO_2 particle contact. Very recently, Gregg et al. reported[31] that the electrical potential in the particulate TiO_2 film was effectively screened over a short range by ionic charges in the electrolyte within the film, but no study has yet been made on the nature of the electrical junction at the TiO_2/substrate interface.

Experimental Section

Three kinds of particulate TiO_2 film electrodes, prepared from colloidal TiO_2 solutions, were used in the present work, together with single-crystal n-TiO_2 (rutile) electrodes. The colloidal TiO_2 solutions were prepared as follows.

Method A. A solution of rutile-type TiO_2 particles was prepared according to a method reported by Fujishima et al.[36] Two milliliters (mL) of titanium tetrachloride ($TiCl_4$, 99.0% in purity, Wako Pure Chemical Industries, Ltd.) was added dropwise to 50 mL of aqueous 1.0 M (M = mol/dm^3) sodium carbonate (Na_2CO_3) under vigorous stirring at 5 °C, followed by addition of 3 mL of 60% nitric acid (HNO_3). The mixture was kept at 75 °C for 4 h under stirring. A surfactant (called Triton X-100) was added to the obtained colloidal solution at a ratio of 1 g per 20 mL of solution in order to avoid precipitation.

Method B. A solution of mainly anatase-type TiO_2 particles was prepared according to the method of Grätzel et al.[37] A mixture of 25 mL of titanium tetra(isopropoxide) ($Ti(OC_3H_7)_4$, 95.0% in purity, Wako Pure Chemical Industries, Ltd.) and 8

* Corresponding author. FAX: +81-6-850-6236. E-mail: nakato@chem.es.osaka-u.ac.jp.

S1089-5647(98)01280-2 CCC: $15.00
Published on Web 07/07/1998

mL of 2-propanol was added to 150 mL of 0.4% HNO_3 under vigorous stirring at 5 °C, and then the solution was kept at 75 °C for 4 h under stirring. A surfactant (Triton X-100) was added to the obtained colloidal solution at a ratio of 0.5 g per 20 mL of solution.

Method C. Commercial TiO_2 powder, called JRC-TIO-4 in the Catalysis Society of Japan, which was essentially the same as Degussa P-25, was used. The powder (2 g) was ground with 4 mL of water and 0.4 mL of acetylacetone in a mortar. The obtained mixture was added to 40 mL of 1.5% HNO_3, followed by addition of Triton X-100 at a ratio of 0.5 g per 20 mL of solution.

Particulate TiO_2 film electrodes were prepared as follows: Transparent conductive F-doped SnO_2 films on glass plates (Nippon Sheet Glass Co. Ltd., sheet resistance ca. 20 Ω/square) and gold and platinum plates were used as the substrates. They were cut into pieces ca. 1.5 × 2.0 cm^2 in area, and washed successively with boiling acetone, 30% HNO_3, and pure water. The colloidal TiO_2 solutions were coated on the substrate with a spin coater at 2000 rpm and heated at 150 °C using an electric furnace. This procedure was repeated several times, and the TiO_2 films thus obtained were finally heated at 600 °C for 2 h in air, the temperature being slowly raised initially at a rate of 100 °C/h. A copper wire was attached on an edge of the substrate with silver paste, and the whole part, except a 1.0 × 1.0 cm^2 TiO_2 film area, was covered with epoxy resin for insulating.

Single-crystal n-TiO_2 (rutile) electrodes were prepared by use of TiO_2 wafers (10 × 10 × 1 mm^3) cut perpendicular to the *c*-axis and having a purity of 99.99%, obtained from Earth Chemical Co., Ltd. They were polished with alumina powder of diameters 3.0, 1.0, 0.3, and 0.06 μm successively, etched in 97% H_2SO_4 containing 33% $(NH_4)_2SO_4$ at 240 °C for 30 min, washed, annealed in air at 1300 °C for 4 h, and then slightly reduced by heating at 680−700 °C for 30 min in a stream of hydrogen for getting n-type semiconductivity.

The current density (*j*)−potential (*U*) curves were obtained with a commercial potentiostat and potential programmer, using a Pt wire (0.5 mm in diameter, 20 mm long) as the counter electrode and an Ag/AgCl/KCl(sat.) electrode as the reference electrode. Electrolyte solutions were prepared using deionized water and reagent grade chemicals without further purification. Illumination was performed with a 300 or 500 W Xe lamp (Ushio) as the light source. In most cases, the light was monochromatized with a monochromator (Jarrel-Ash JE-25E) and chopped at 0.5 Hz with a chopper (Scitec Instruments Ltd., 300HRG) in order to distinguish photocurrents and dark currents clearly. The intensity of monochromatic light at 340 nm (where TiO_2 gives the highest photocurrent) was 0.38 mW/cm^2 as measured with a thermopile (Eppley). The illumination area was 1.0 × 1.0 cm^2, the same as the aforementioned active TiO_2 film area. Nitrogen gas was bubbled through the electrolyte before and during experiments in order to remove dissolved oxygen.

Inspection of electrode structure was carried out with a high-resolution scanning electron microscope (Hitachi S-5000). X-ray diffraction patterns were obtained with a Philips X'Pert diffractometer using a Cu Kα radiation (λ = 1.5417 Å).

Results

Hereafter, particulate TiO_2 films (or electrodes) obtained from the colloidal TiO_2 solutions prepared by methods A, B, and C (see the Experimental Section) are called film A, B, and C (or electrode A, B, and C), respectively. Figure 1 shows scanning electron micrographs of film A on a gold substrate and film B on an SnO_2 substrate. Both the films consist of particles 10−30 nm in diameter. Film C also consists of particles of nearly the same size. The thickness of films A and B is 250−350 nm, and that of film C is ca. 1.2 μm.

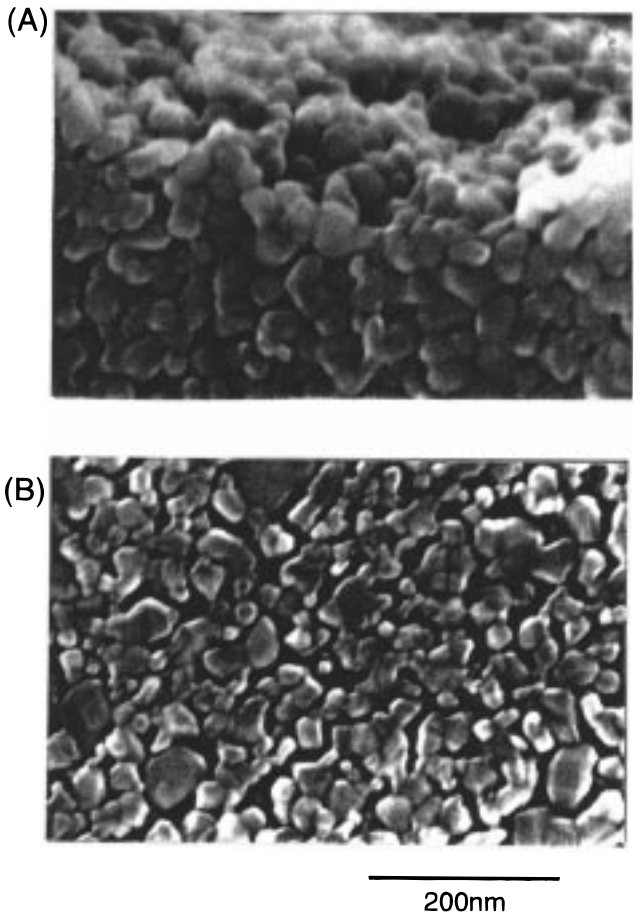

Figure 1. Scanning electron micrographs of particulate TiO_2 films: (A) inclined view of film A on a gold substrate and (B) top view of film B on an SnO_2 substrate.

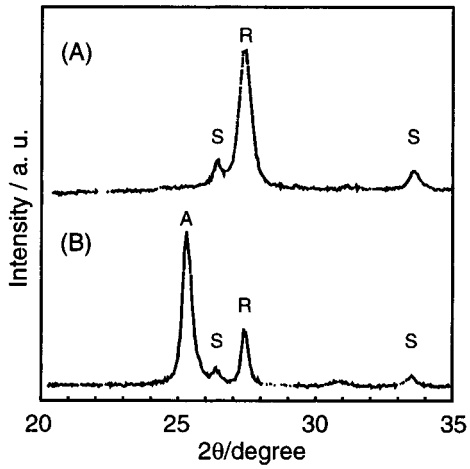

Figure 2. X-ray diffraction patterns of particulate TiO_2 films: (A) for film A and (B) for film B, both deposited on SnO_2 substrates. R = rutile peak, A = anatase peak, and S = peaks assigned to the SnO_2 substrate.

Figure 2 shows X-ray diffraction patterns for films A and B, both deposited on SnO_2 substrates. Film A shows only a rutile-type TiO_2 peak at 2θ = 27.6°, apart from peaks assigned to the SnO_2 substrate, indicating that film A consists of 100% rutile-

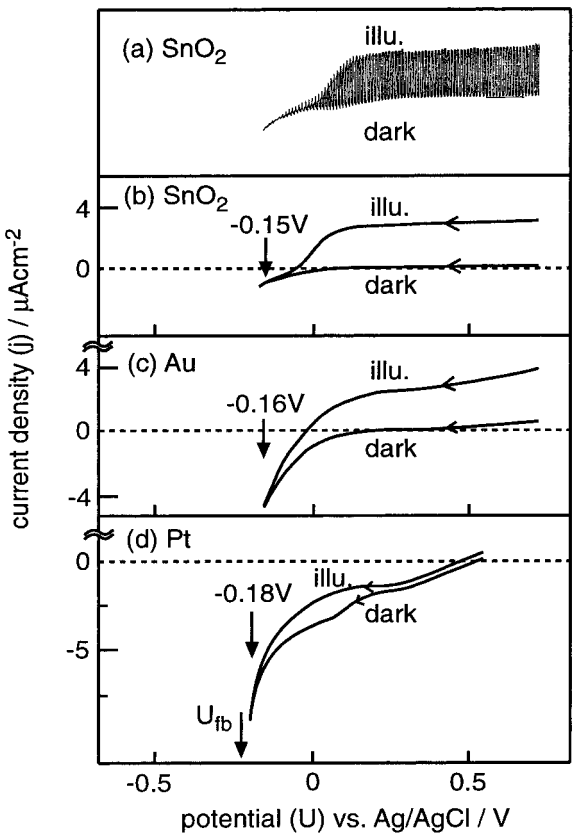

Figure 3. Current density−potential curves for particulate TiO_2 film electrodes of 100% rutile-type (electrode A) prepared on various substrates (SnO_2, Au, and Pt) in 0.1 M $HClO_4$ (pH 1.1): (a) an actually observed curve under chopped illumination at 340 nm on a negative scan and (b) curves in the dark and under illumination, obtained from curve a. Curves c and d are obtained similar to curve b. U_{on} is the onset potential of photocurrent. U_{fb} is the flat-band potential of single-crystal n-TiO_2 (rutile) electrodes reported[42−44] at pH 1.1.

type TiO_2 particles. On the other hand, film B shows a strong anatase-type TiO_2 peak at $2\theta = 25.4°$ and a weak rutile-type TiO_2 peak, from which the film is calculated to consist of 83% anatase-type and 17% rutile-type particles. The particle size was calculated from the peak width and Scherrer's equation[38] to be 18 nm for film A and 25 nm for film B, in agreement with the size obtained from the SEM's (Figure 1). Similar experiments have shown that film C consists of 70% anatase-type and 30% rutile-type particles, the particle size being 30 nm.

Figure 3 shows current density (j)−potential (U) curves for particulate TiO_2 electrodes of 100% rutile-type (electrode A) prepared on various substrates. The electrolyte is 0.1 M $HClO_4$ (pH 1.1). For the SnO_2 substrate (Figure 3a,b), the dark cathodic current starts to flow at ca. +0.05 V vs Ag/AgCl, but for the Au and Pt substrates (Figure 3c,d), it starts at more positive potentials (ca. +0.20 V for Au and ca. +0.50 V for Pt). This is most probably because the electrolyte penetrates into the particulate TiO_2 films and is in direct contact with the substrate, and consequently the dark cathodic current includes a current flowing at the substrate/electrolyte interface. The most positive onset of the cathodic current for the Pt substrate can be attributed to effective reduction of a small amount of molecular oxygen remaining in the electrolyte. Sharp increases in the cathodic current near −0.20 V for the Pt (and Au) substrates are attributed to efficient hydrogen evolution on the substrates. The dark current−potential curve for the Pt substrate shows another cathodic-current shoulder around +0.2 V, the origin of which

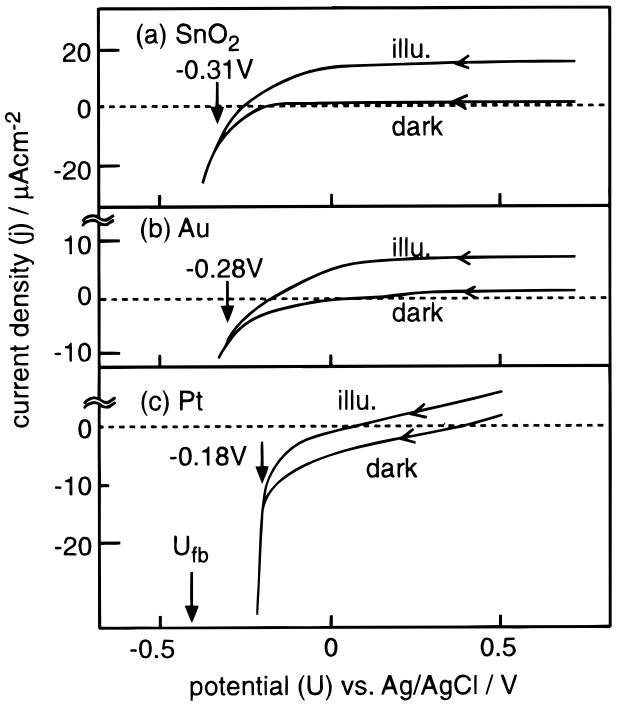

Figure 4. Current density−potential curves for particulate TiO_2 electrodes of mainly anatase-type (electrode B) on various substrates (SnO_2, Au, and Pt) in 0.1 M $HClO_4$ (pH 1.1). U_{fb} is the flat-band potential of single-crystal n-TiO_2 (anatase) electrodes reported[41] at pH 1.1.

is unknown yet. Anyway, the photocurrent can be distinguished from the dark current by use of chopped illumination, and the onset potential of photocurrents (U_{on}) is determined precisely.

From Figure 3, it is clear that the U_{on} is nearly the same among the SnO_2, Au, and Pt substrates, though the work functions ($e\phi_w$) of the substrates, which are reported to be 4.85, 5.10, and 5.60 eV, respectively,[39,40] are largely different from each other. Figure 3 shows the $j-U$ curve on negative scans for simplicity, but positive scans give nearly the same $j-U$ curve, the U_{on} for both scans agreeing within a range of ±0.02 V.

Similar experiments were done for other particulate TiO_2 electrodes (electrodes B and C) of mainly anatase type in order to confirm the generality of the above conclusion. The results are shown in Figures 4 and 5. The U_{on} values for the SnO_2 and Au substrates are nearly the same as each other, similar to the case of Figure 3. It is to be noted that the U_{on} for the SnO_2 and Au substrates in Figures 4 and 5 are ca. 0.15 V more negative than the U_{on} in Figure 3. This is most probably attributed to the fact that the reported flat-band potential (U_{fb}) for anatase-type TiO_2[41] (−0.16 V vs NHE at pH 0) is ca. 0.15 V more negative than that for rutile-type[42−44] (0.00−0.05 V vs NHE at pH 0). The U_{on} for the Pt substrate in Figures 4 and 5 lies more positive than those for the SnO_2 and Au substrates, which is attributed to sharply increasing hydrogen evolution cathodic currents on the Pt substrate at around −0.20 V.

Table 1 summarizes the U_{on} values for various electrodes, various substrates, and various solutions. The U_{on} values for a single-crystal n-TiO_2 (rutile) electrode are also included for comparison. The U_{on} is independent of the work function of the substrate, irrespective of whether ethanol is present or not in the solutions. The more positive U_{on} for the Pt substrate than those for the SnO_2 and Au substrates, observed for electrode A in a solution with ethanol and for electrodes B and C, are

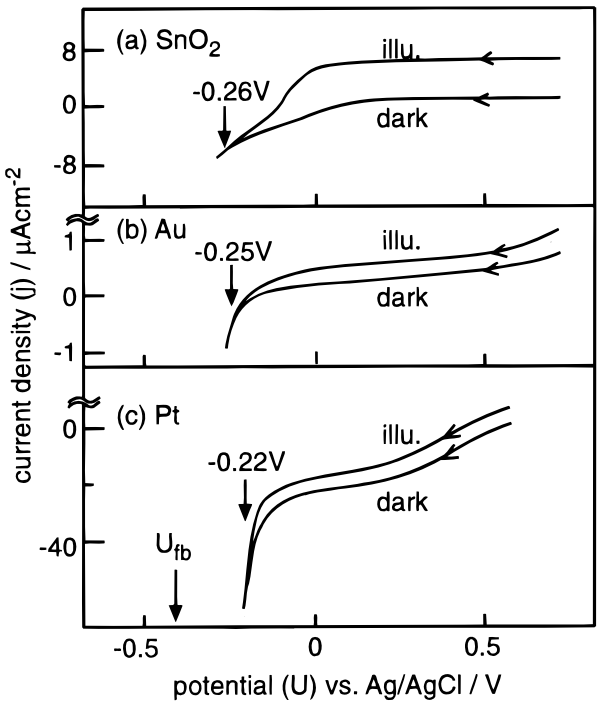

Figure 5. Current density−potential curves for particulate TiO_2 (P-25) electrodes of mainly anatase-type (electrode C) on various substrates (SnO_2, Au, and Pt) in 0.1 M $HClO_4$ (pH 1.1). U_{fb} is the same as in Figure 4.

TABLE 1: Onset Potentials of Photocurrents (U_{on}), in Units of V vs Ag/AgCl, for Various Particulate TiO_2 Film Electrodes on Various Substrates in 0.1 M $HClO_4$ (pH 1.1) with and without Ethanol, Together with Those for a Single-Crystal n-TiO_2 (rutile) Electrode

		substrate		
electrode	solution 0.1 M $HClO_4$ with	SnO_2 (4.85 eV)[a]	Au (5.1 eV)[a]	Pt (5.6 eV)[a]
electrode A	no EtOH	−0.15	−0.16	−0.18
	0.34 M EtOH	−0.30	−0.29	−0.19
electrode B	no EtOH	−0.31	−0.28	−0.18
	0.34 M EtOH	−0.36	−0.37	−0.23
electrode C	no EtOH	−0.26	−0.25	−0.22
	0.34 M EtOH	−0.35	−0.33	−0.25
single crystal n-TiO_2 (rutile)	no EtOH		−0.13	
	0.34 M EtOH		−0.27	

[a] The work functions ($e\phi_w$) of the substrates (SnO_2, Au, and Pt) reported.[39,40]

attributed to the effect of efficient hydrogen evolution on the Pt substrate as already mentioned.

Figure 6 shows the effect of solution pH on the $j-U$ curves for electrodes A, B, and C in the absence and presence of ethanol, together that for a single-crystal n-TiO_2 (rutile) electrode.[32−34] The particulate TiO_2 electrodes show the $j-U$ curves similar to those for single-crystal n-TiO_2. It is to be noted that, in the absence of ethanol (solid lines), the deviation (ΔU) of U_{on} from U_{fb} ($\Delta U = U_{on} - U_{fb}$) in acidic solution is considerably larger than that in alkaline solution. The ΔU becomes nearly zero when ethanol is added to the solutions (broken curves). The saturated photocurrent (j_{sat}) for the particulate TiO_2 electrodes in alkaline solution is in general higher than that in acidic solution. The j_{sat} is much enhanced by addition of ethanol.

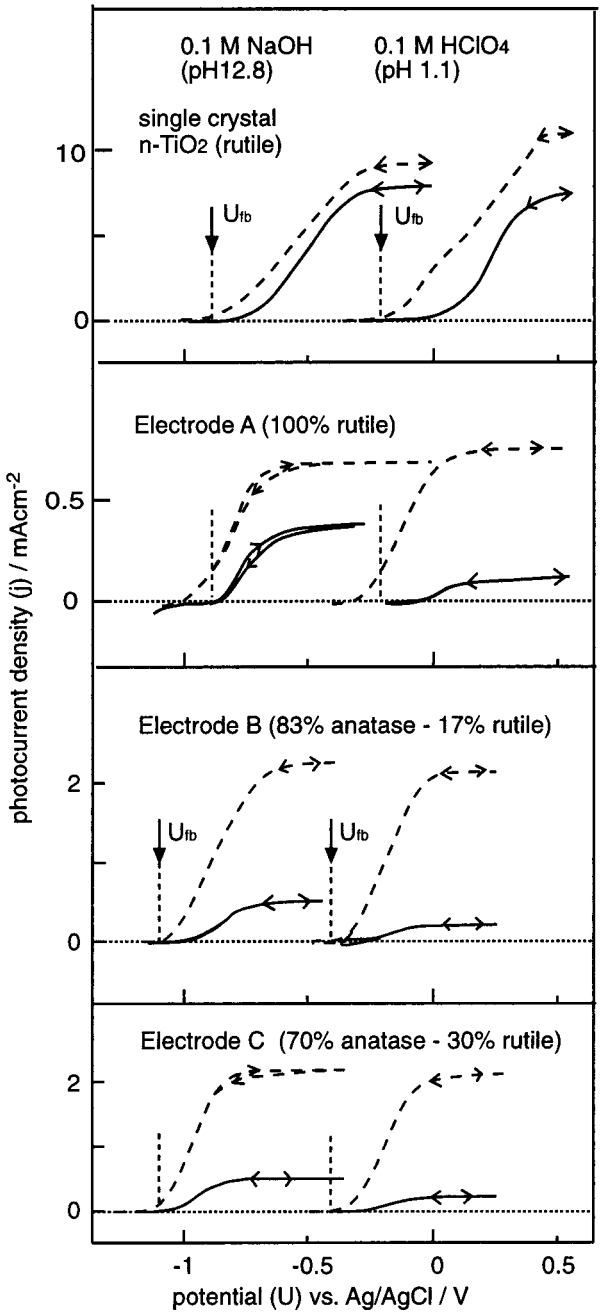

Figure 6. Effect of solution pH on the $j-U$ curves for electrodes A, B, and C prepared on the SnO_2 substrates in the absence (solid curves) and the presence (broken curves) of 0.31 M ethanol, together with those for a single-crystal n-TiO_2 (rutile) electrode, obtained under continuous white light illumination with a 500 W Xe lamp (0.94 W cm^{-2}). U_{fb} is the flat-band potentials of single-crystal n-TiO_2 electrodes of rutile[42−44] (for electrode A) and anatase type[41] (electrodes B and C) reported.

Discussion

We can conclude from Figures 3−5 and Table 1 that the onset potentials of photocurrents (U_{on}) for particulate TiO_2 film electrodes remain nearly the same, irrespective of the work function ($e\phi_w$) of the substrate. The conclusion holds for all the particulate TiO_2 electrodes and all the solutions irrespective of whether ethanol is added or not, if the effect of the sharply increasing hydrogen-evolution cathodic current on the Pt substrate at around −0.20 V is taken into account as mentioned before.

The U_{on} value in the present work, determined from the point of divergence of the $j-U$ curves in the dark and under

illumination, may be affected by flow of a dark cathodic current as mentioned above for the Pt substrate. The U_{on} may also be affected by a change in the photocurrent density (or illumination intensity) and by charge-carrier recombination at the TiO_2 surface. However, the aim of the present work is not to determine the U_{on} itself precisely but to determine the relative shift in U_{on} by the change of the work function ($e\phi_w$) of the substrate. Thus, the present experiments were done under the same illumination condition and the same current density scale together with the same optical arrangement of the cell and TiO_2 electrode in order to minimize a scattering of the U_{on} value. In fact, the observed scattering of U_{on} among various substrates is less than 0.04 V, except for relatively large differences of 0.10−0.14 V between the SnO_2 and Pt substrates (Table 1). This is much smaller than the difference in the work function ($e\phi_w$) of the substrate, which reaches 0.25 eV between SnO_2 and Au and 0.75 eV between SnO_2 and Pt.[39,40] Thus, the above conclusion that the U_{on} is independent of the work function ($e\phi_w$) of the substrate is unambiguous.

Now let us consider some plausible models for the electrical junction at the TiO_2 particle/substrate interface in order to explain the above conclusion. Figure 7A shows a conventional Schottky junction model, which is most frequently assumed for metal/metal oxide semiconductor contacts. In this model, the TiO_2 particle and substrate are in contact with each other with no change in the surface chemical structure by contact, and thus the barrier height at the interface ($e\Phi_B$) is given by the energy difference between the conduction band edge of the TiO_2 particle at the surface, $E_c^s(TiO_2)$, and the Fermi level of the substrate, E_F(subs), before contact. Since E_F(subs) is equal to $-e\phi_w$ (negative of the work function),

$$e\Phi_B = E_c^s(TiO_2) - E_F(subs) = E_c^s(TiO_2) + e\phi_w \quad (1)$$

In the case where the TiO_2/substrate contact (particulate TiO_2 electrode) is in an aqueous electrolyte, the conduction-band edge of the TiO_2 particle at the TiO_2/solution interface, $E_c^s(TiO_2,sol)$ (cf. Figure 7A), is determined by solution pH[45] and remains constant for a given solution. The Fermi level of the substrate, E_F(subs), is determined by the electrode potential (U) and given as

$$E_F(subs) = -eU + E_{F,ref} \quad (2)$$

where $E_{F,ref}$ is the Fermi level of the reference electrode which can be regarded as a constant quantity. Since the barrier height $e\Phi_B$ is also constant for a Schottky junction model, independent of U, the conduction-band edge of the TiO_2 particle at the TiO_2/substrate interface, $E_c^s(TiO_2,subs)$ (cf. Figure 7A), changes with U by the following equation:

$$E_c^s(TiO_2,subs) = E_F(subs) + e\Phi_B = -eU + E_{ref} + e\Phi_B \quad (3)$$

Thus, $E_c^s(TiO_2,subs)$ change with U, whereas $E_c^s(TiO_2,sol)$ remains constant as mentioned above, and band inclination is induced in the TiO_2 particle with the shift in U. This band inclination is different in nature from a so-called "band bending" for a semiconductor electrode, because the TiO_2 particle in the present work is an insulator.

What $j-U$ curve is expected from the above Schottky junction model? Let us first define the critical electrode potential U_{cr} at which $E_c^s(TiO_2,subs)$ equals $E_c^s(TiO_2,sol)$ (cf. Figure 7A). When $U > U_{cr}$, upward band inclination ($E_c^s(TiO_2,subs) < E_c^s(TiO_2,sol)$) is induced in the TiO_2 particle, and an anodic photocurrent flows under illumination. Thus, we can expect that a photoanodic current starts at $U = U_{cr}$ and becomes constant at $U \gg U_{cr}$. For the Schottky junction model of Figure 7A, U_{cr} (and hence U_{on}) depend on $e\Phi_B$, namely $e\phi_w$, which is in disagreement with the experiments (Table 1).

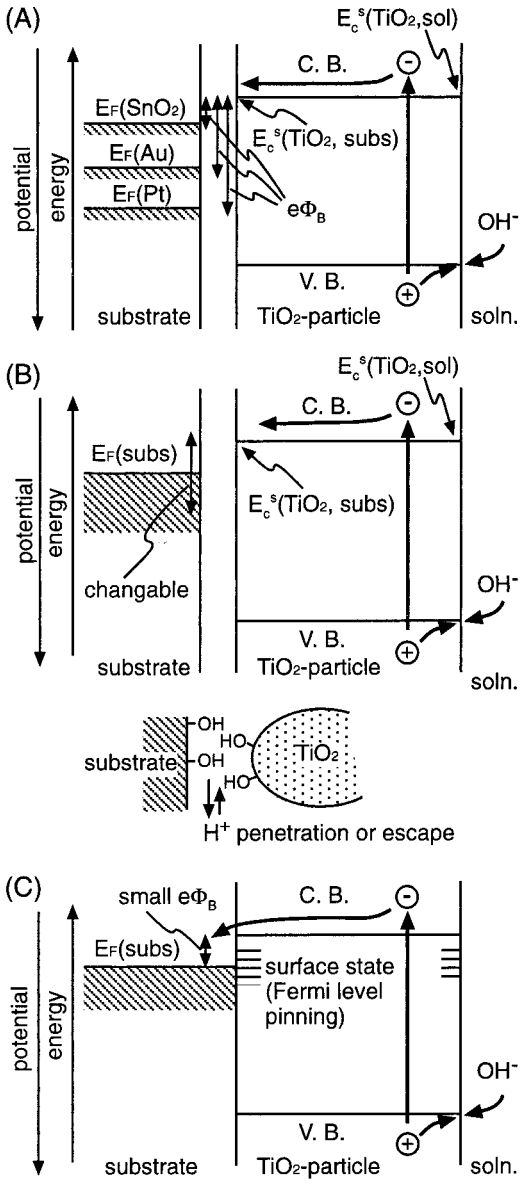

Figure 7. Three plausible models for the electrical junction at the TiO_2 particle/substrate interface: (A) a Schottky junction model, (B) an extended Schottky junction model, and (C) a Bardeen-type junction model. C. B. = conduction band, V. B. = valence band, (−) = electron, and (+) = hole. See text for other details.

Next, let us consider another model such as shown in Figure 7B, which can explain the experimental result that U_{on} does not depend on $e\phi_w$ (Table 1). In the above Schottky junction model, it is assumed that no change in the surface chemical structure occurs at the TiO_2/substrate interface, and thus $e\Phi_B$ is kept constant, independent of U. If we assume that ions such as H^+ and OH^- can penetrate into (or escape from) the TiO_2/substrate interface as shown in the lower part of Figure 7B, electrical double layers are formed at the TiO_2 and substrate surfaces, and E_F(subs) can change freely, independent of $E_c^s(TiO_2,subs)$, which is equal to $E_c^s(TiO_2,sol)$ in the present model. A similar free change of E_F(subs) with respect to $E_c^s(TiO_2,subs)$ may be expected if the area of direct contact between the TiO_2 particles and the substrate is very small, say, $\leq 1-2$ nm^2,

because an electrical screening effect similar to that mentioned above will be achieved by ions in the electrolyte surrounding the direct-contact area.[31,46−48] In this model, which may be called an "extended Schottky junction" model, the bands of the TiO_2 particle are always flat, independent of U, and an anodic photocurrent can flow when E_F(subs) is below $E_c^s(TiO_2,subs)$. Namely, the photocurrent onset (U_{on}) is determined by $E_c^s(TiO_2,subs) = E_c^s(TiO_2,sol)$ and becomes independent of $e\phi_w$.

However, there is another experimental result that is difficult to explain by the model of Figure 7B. As shown in Figure 6, in the absence of ethanol (solid lines), the deviation (ΔU) of U_{on} from U_{fb} in acidic solution (ca. 0.3 V) is considerably larger than that in alkaline solution (ca. 0.1 V). The deviations in both solutions become nearly zero when ethanol is added to the solutions. Though the saturated photocurrent (j_{sat}) in the $j-U$ curve is different in different solutions and this difference in j_{sat} may affect the ΔU to some extent, the observed differences in ΔU between the acidic and alkaline solutions (or between the presence and absence of ethanol) are larger than expected from the difference in j_{sat}, as confirmed experimentally by changing the illumination intensity.

Single-crystal n-TiO_2 electrodes show similar differences in ΔU among various solutions (uppermost curves in Figure 6), which were explained in previous papers[33,34] as follows: The surface Ti−OH group on a TiO_2 crystal cannot be oxidized by photogenerated holes, and thus, in acidic solutions, Ti−OH in certain active sites such as atomic gaps exposed to the surface is oxidized by holes. The resultant Ti·OH radicals in the atomic gaps, present more or less deep below the surface, induce efficient electron−hole recombination. Thus, a photocurrent can flow only when certain band bending is formed by a positive shift of the electrode potential. This leads to a large deviation (ΔU). In alkaline solutions, deprotonated surface species such as $Ti-O^-$ are produced and oxidized by holes. The resultant surface radicals (Ti−O·) are more mobile than the Ti·OH radicals in the atomic gaps and hence easily removed from the surface through formation of hydrogen peroxide and oxygen evolution, resulting in a low density of surface intermediate radicals and hence less surface carrier recombination. In the presence of ethanol, adsorbed ethanol ($Ti-OC_2H_5$) is formed and oxidized efficiently by holes by a current-doubling mechanism[49] (electron injection into the conduction band of n-TiO_2 from intermediate ethoxy radicals produced by hole oxidation). This mechanism leads to a further low density of surface intermediate radicals and hence much less surface carrier recombination. In short, the deviation ΔU is determined by surface carrier recombination via surface intermediate radicals produced by hole oxidation.

A similar mechanism to the above for single-crystal n-TiO_2 is expected for particulate TiO_2 electrodes. It is to be noted first that almost no deviation ΔU for the particulate TiO_2 electrodes in the presence of ethanol (broken lines in Figure 6), which will be caused by a low density of surface intermediate radicals and hence a small rate of surface carrier recombination, indicates that the conduction-band edge at the TiO_2 particle surface, $E_c^s(TiO_2)$, lies nearly the same as that for single-crystal n-TiO_2 electrodes. The $E_c^s(TiO_2)$ is solely determined by solution pH and independent of whether ethanol is present or not, as mentioned before. Thus, the large deviation ΔU in acidic solution without ethanol (Figure 6) implies that a photocurrent starts to flow when the electrode potential (or the Fermi level of the substrate) is shifted downward to some extent from U_{fb} (or $E_c^s(TiO_2)$). This can be explained by considering that certain band inclination (or band bending) is formed in some TiO_2 particles by the shift of the electrode potential, and surface carrier recombination is suppressed. The formation of band inclination cannot be explained by the model of Figure 7B.

Thus, we finally propose a model of Figure 7C that can explain all the experimental results. In this model, we assume that a certain reductive surface state such as Ti^{3+} is formed near the conduction-band edge of TiO_2, $E_c^s(TiO_2)$, under illumination, as reported.[50−53] Such a reductive surface state will cause Fermi level pinning (the agreement of the Fermi level of the surface state and that of the substrate) at the TiO_2 particle/substrate interface. The junction of such a type is sometimes called Bardeen-type junction.[54] If the Fermi level of the surface state lies near $E_c^s(TiO_2)$ as mentioned above, the barrier height ($e\Phi_B$) of the junction is low. Thus, an electrical junction like "ohmic contact with an n-TiO_2 semiconductor" is formed at the TiO_2 particle/substrate interface (see Figure 7C), and we can expect that the particulate TiO_2 electrode behaves like a single-crystal n-TiO_2 electrode, in agreement with the experiments.

In conclusion, we have considered three models for the electrical junction at the TiO_2 particle/substrate interface. Of these, the models of Figure 7B,C can explain the U_{on} values independent of the work function of the substrate, but only the model of Figure 7C can explain the changes in the deviation (ΔU) by change of solution pH and addition of alcohol. However, the model of Figure 7B cannot be excluded at present because the observed changes in ΔU may not necessarily be large enough to derive a definite conclusion. Moreover, there remains a possibility that the models of Figure 7B,C are mixed at actual interfaces even though the latter may be dominant. Further studies are necessary to clarify more details on the nature of the electrical junction at the interface.

Acknowledgment. This work was partly supported by Grant-in-Aid for Scientific Research on Priority Area of "Electrochemistry of Ordered Interfaces" (No. 09237105) from the Ministry of Education, Science, Sports and Culture, Japan.

References and Notes

(1) Fujishima, A.; Honda, K. *Nature* **1972**, *238*, 37.
(2) *Photocatalytic Purification and Treatment of Water and Air*; Ollis, D. F., Al-Ekabi, H., Eds.; Elsevier: Amsterdam, 1993.
(3) *Semiconductor Nanoclusters*; Kamat, P. V., Meisel, D., Eds.; Studies in Surface Science and Catalysis 103; Elsevier: Amsterdam, 1996.
(4) Cai, R.; Hashimoto, K.; Itoh, K.; Kubota, Y.; Fujishima, A. *Bull. Chem. Soc. Jpn.* **1991**, *64*, 1268.
(5) Ikeda, K.; Sakai, H.; Baba, R.; Hashimoto, K.; Fujishima, A. *J. Phys. Chem. B* **1997**, *101*, 2617.
(6) Fox, M. A.; Dulay, M. T. *Chem. Rev.* **1993**, *93*, 341.
(7) Minero, C.; Pelizzetti, E.; Terzian, R.; Serpone, N. *Langmuir* **1994**, *10*, 692.
(8) Hoffmann, M. R.; Martin, S. T.; Choi, W.; Bahnemann, D. W. *Chem. Rev.* **1995**, *95*, 69.
(9) Linsebigler, A. L.; Lu, G.; Yates, J. T., Jr. *Chem. Rev.* **1995**, *95*, 735.
(10) Schwitzgebal, J.; Ekerdt, J. G.; Gerischer, H.; Heller, A. *J. Phys. Chem.* **1995**, *99*, 5633.
(11) Sclafani, A.; Herrmann, J. M. *J. Phys. Chem.* **1996**, *100*, 13655.
(12) Yamashita, H.; Ichihashi, Y.; Harada, M.; Stewart, G.; Fox, M. A.; Anpo, M. *J. Catal.* **1996**, *158*, 97.
(13) Takeda, N.; Ohtani, M.; Torimoto, T.; Kuwabata, S.; Yoneyama, H. *J. Phys. Chem. B* **1997**, *101*, 2644.
(14) Ohtani, B.; Iwai, K.; Nishimoto, S.; Sato, S. *J. Phys. Chem. B* **1997**, *101*, 3349.
(15) Bahnemann, D. W.; Hilgendorff, M.; Memming, R. *J. Phys. Chem. B* **1997**, *101*, 4265.
(16) Hagfeldt, A.; Grätzel, M. *Sol. Energy Mater. Sol. Cells* **1994**, *32*, 243.
(17) Södergren, S.; Hagfeldt, A.; Olsson, J.; Lindquist, S.-E. *J. Phys. Chem.* **1994**, *98*, 5552.
(18) Cao, F.; Oskam, G.; Searson, P. C.; Stipkala, J. M.; Heimer, T. A.; Farzad, F.; Meyer, G. J. *J. Phys. Chem.* **1995**, *99*, 11974.

(19) Wahl, A.; Ulmann, M.; Carroy, A.; Jermann, B.; Dolata, M.; Kedzierzawski, P.; Chatelain, C.; Monnier, A.; Augustynski, J. *J. Electroanal. Chem.* **1995**, *396*, 41.
(20) Rensmo, H.; Lindström, H.; Södergren, S.; Willstedt, A.-K.; Hagfeldt, A.; Lindquist, S.-E. *J. Electrochem. Soc.* **1996**, *143*, 3173.
(21) Zhou, M.; de Tacconi, N. R.; Rajeshwar, K. *J. Electroanal. Chem.* **1997**, *421*, 111.
(22) Boschloo, G. K.; Goossens, A.; Schoonman, J. *J. Electroanal. Chem.* **1997**, *428*, 25.
(23) de Jongh, P. E.; Vanmaekelbergh, D. *J. Phys. Chem. B* **1997**, *101*, 2716.
(24) O'Regan, B.; Grätzel, M. *Nature (London)* **1991**, *335*, 737.
(25) Willig, F.; Eichberger, R.; Sundaresan, N. S.; Parkinson, B. A. *J. Am. Chem. Soc.* **1990**, *112*, 2702.
(26) Kamat, P. V. *Chem. Rev.* **1993**, *93*, 267.
(27) Hagfeldt, A.; Grätzel, M. *Chem. Rev.* **1995**, *95*, 49.
(28) Murakoshi, K.; Kano, G.; Wada, Y.; Yanagida, S.; Miyazaki, H.; Matsumoto, M.; Murasawa, S. *J. Electroanal. Chem.* **1995**, *396*, 27.
(29) Grünwald, R.; Tributsch, H. *J. Phys. Chem. B* **1997**, *101*, 2564.
(30) Schlichthörl, G.; Huang, S. Y.; Sprague, J.; Frank, A. J. *J. Phys. Chem. B* **1997**, *101*, 8141.
(31) Zaban, A.; Meier, A.; Gregg, B. A. *J. Phys. Chem. B* **1997**, *101*, 7985.
(32) Nakato, Y.; Akanuma, H.; Shimizu, J.-I.; Magari, Y. *J. Electroanal. Chem.* **1995**, *396*, 35.
(33) Magari, Y.; Ochi, H.; Yae, S.; Nakato, Y. *ACS Symposium Series No. 656* (Solid/Liquid Electrochemical Interfaces); American Chemical Society: Washington, DC, 1996; Chapter 21, p 297.
(34) Nakato, Y.; Akanuma, H.; Magari, Y.; Yae, S.; Shimizu, J.-I.; Mori, H. *J. Phys. Chem. B* **1997**, *101*, 4934.
(35) Marcus, R. A. *Annu. Rev. Phys. Chem.* **1964**, *15*, 155.
(36) Sopyan, I.; Watanabe, M.; Murasawa, S.; Hashimoto, K.; Fujishima, A. *Chem. Lett.* **1996**, 69.
(37) O'Regan, B.; Moser, J.; Anderson, M.; Grätzel, M. *J. Phys. Chem.* **1990**, *94*, 8720.
(38) Scherrer, P. *Nachr. Kgl. Ges. Wiss. Gottingen Math.-phys. Kl.* **1918**, 98.
(39) Nanthakumar, A.; Armstrong, N. R. In *Semiconductor Electrodes;* Finklea, H. O., Ed.; Elsevier: Amsterdam, 1988; Studies in Physical and Theoretical Chemistry 55, pp 203−239.
(40) Eastman, D. E. *Phys. Rev. B* **1970**, *2*, 1.
(41) Kavan, L.; Grätzel, M.; Gilbert, S. E.; Klemenz, C.; Scheel, H. J. *J. Am. Chem. Soc.* **1996**, *118*, 6716.
(42) Gandia, J.; Pujadas, M.; Salvador, P. *J. Electroanal. Chem.* **1988**, *244*, 69.
(43) Tomkiewicz, M. J. *J. Electrochem. Soc.* **1979**, *126*, 1505.
(44) Finklea, H. O. *Semiconductor Electrodes;* Finklea, H. O., Ed.; Elsevier: Amsterdam, 1988; Studies in Physical and Theoritical Chemistry 55, pp 43−145.
(45) Yates, D. E.; James, R. O.; Hearly, T. W. *J. Chem. Soc., Faraday Trans. 1* **1980**, *76*, 1.
(46) Nakato, Y.; Ueda, K.; Yano, H.; Tsubomura, H. *J. Phys. Chem.* **1988**, *92*, 2316.
(47) Nakato, Y.; Tsubomura, H. *Electrochim. Acta* **1992**, *37*, 897.
(48) Jia, J. G.; Fujitani, M.; Yae, S.; Nakato, Y. *Electrochim. Acta* **1996**, *42*, 431.
(49) Morrison, S. R.; Freund, T. *J. Chem. Phys.* **1967**, *47*, 1563.
(50) Sanjinés, R.; Tang, H.; Berger, H.; Gozzo, F.; Margaritondo, G.; Lévy, F. *J. Appl. Phys.* **1994**, *75*, 2945.
(51) Gufierrez, C.; Salvador, P. *J. Electroanal. Chem.* **1982**, *138*, 457.
(52) Howe, R. F.; Grätzel, M. *J. Phys. Chem.* **1985**, *89*, 4495.
(53) Rajh, T.; Ostafin, A. E.; Micic, O. I.; Tiede, D. M.; Thurnauer, M. *J. Phys. Chem.* **1996**, *100*, 4538.
(54) Sze, S. M. *Physics of Semiconductor Devices*; John Wiley & Sons: New York, 1981; Chapter 5.